Supporting Information

Electronic structure and slow magnetic relaxation of low-coordinate cyclic alkyl(amino) carbene stabilized iron (I) complexes

Prinson P. Samuel,[1] Kartik Chandra Mondal,[1] Nurul Amin Sk,[1] Herbert W. Roesky,[1]* Elena Carl,[1] Roman Neufeld,[1] Dietmar Stalke,[1]* Serhiy Demeshko,[1] Franc Meyer,[1]* Liviu Ungur,[2]* Liviu F. Chibotaru,[2] Jonathan Christian,[3] Vasanth Ramachandran,[3] Johan van Tol[4] and Naresh S. Dalal[3,4]*

[1]*Institut für Anorganische Chemie, Georg-August-Universität, Tammannstrasse 4, D-37077, Göttingen, Germany.*

[2] *KU Leuven, Celestijnenlaan, 200F, 3001, Leuven, Belgium.*

[3]*Departments of Chemistry and Biochemistry, Florida State University, Tallahassee, FL 32306, USA.*

[4]*National High Magnetic Field Laboratory, Florida State University, Tallahassee, FL 32306, USA.*

Contents:

S1. Crystallographic information

Crystal Structure Determination

Suitable single crystals were selected from the mother liquor in the Schlenk flask and covered with perfluorinated polyether oil on a microscope slide, which was cooled with a nitrogen gas flow using the X-Temp2 device.[S1] The diffraction data of **2** and **3** were collected at 100 K on a Bruker D8 three circle diffractometer equipped with a SMART APEX II CCD detector and a microfocus source[S2] with INCOATEC Quazar mirror-monochromated Mo-Kα radiation (λ = 0.71073 Å **2**) and mirror-monochromated Ag-Kα radiation (λ = 0.56086 Å **3**) and the data for **1** on a Bruker TXS-Mo rotating anode with mirror optics and a Smart Apex II Ultra detector. The data were integrated with SAINT[S3] and a multi-scan absorption correction with SADABS[S4] was applied. The structures were solved by direct methods (SHELXS-97)[S5a] and refined against all data by full-matrix least-squares methods on F^2 (SHELXL2013)[S5b,c] within the SHELXLE GUI.[S5d] The hydrogen atoms were refined isotropically on calculated positions using a riding model with their U_{iso} values constrained to 1.5 U_{eq} of their pivot atoms for terminal sp^3 carbon atoms and 1.2 times for all other carbon atoms. All non-hydrogen-atoms were refined with anisotropic displacement parameters. Disordered moieties were refined using distance restraints and anisotropic displacement parameter restraints (SIMU, RIGU and SAME).[S5c]

Table S1. Crystal and structure refinement parameters for compounds **1-3**.

Parameters	**1**	**2**	**3·(C_6H_5F)**
Empirical formula	$C_{40}H_{62}Cl_2FeN_2$	$C_{40}H_{62}ClFeN_2$	$C_{70}H_{67}BF_{21}FeN_2$
Formula Weight	697.66	662.21	1401.91
Crystal system	monoclinic	monoclinic	triclinic
Space group	*P* 21/*c*	*P* 21/*c*	$P\bar{1}$
Unit cell dimensions	*a* = 13.173(2) Å *b* = 17.403(2) Å *c* = 17.237(2) Å α = 90 ° β = 108.58(2) ° γ = 90 °	*a* = 11.224(2) Å *b* = 19.524(3) Å *c* = 16.903(2) Å α = 90 ° β = 97.29(2) ° γ = 90 °	*a* = 13.666(2) Å *b* = 15.211(2) Å *c* = 18.071(3) Å α = 68.51(2) ° β = 89.00(2) ° γ = 68.72(2) °
Volume, Z	3745.6(9) $Å^3$, 4	3674.1(8) $Å^3$, 4	3228.0(10), 2
Density (calcd)	1.237 Mg/m^3	1.197 Mg/m^3	1.442 Mg/m^3
Absorption coefficient	0.575 mm^{-1}	0.512 mm^{-1}	0.184 mm^{-1}
F (000)	1504	1436	1442
Crystal size/mm	0.10 x 0.08 x 0.06	0.10 x 0.09 x 0.05	0.12 x 0.10 x 0.06
θ range for data collection	1.631 to 26.029 °	1.601 to 27.491 °	1.491 to 19.829
Limiting indices	$-16\le h\le 16, -21\le k\le 21, -21\le l\le 21$	$-14\le h\le 14, -25\le k\le 25, -21\le l\le 21$	$-16\le h\le 16, -18\le k\le 18, -21\le l\le 21$

Reflections collected	107288	110950	111967
Independent reflections	7385 (R_{int} = 0.0622)	8434 (R_{int} = 0.0377)	11911 (R_{int} = 0.0553)
Completeness to θ	100 %(θ = 25.242 °)	99.9 %(θ = 25.242 °)	99.9 %(θ = 19.665 °)
Refinement method	Full-matrix least-squares on F^2	Full - matrix least - squares on F^2	Full - matrix least - squares on F^2
Data/restraints/ parameters	7385 / 0 / 422	8434 / 124 / 413	11911 / 554 / 958
Goodness - of - fit on F^2	1.033	1.031	1.024
Final R indices [$I>2\sigma(I)$]	$R1$ = 0.0317, $wR2$ = 0.0715	$R1$ = 0.0300, $wR2$ = 0.0715	$R1$ = 0.0320, $wR2$ = 0.0707
R indices (all data)	$R1$ = 0.0431, $wR2$ = 0.0764	$R1$ = 0.0338, $wR2$ = 0.0733	$R1$ = 0.0463, $wR2$ = 0.0767
Largest diff. peak and hole	0.373 and -0.325 e.Å^{-3}	0.367 and -0.288 e.Å^{-3}	0.328 and -0.409 e.Å^{-3}

Molecular structure of 1

Compound **1** was crystallized from a saturated solution in toluene at 0 °C. **1** crystallizes in the monoclinic space group $P\,2_1/c$. The coordination geometry around Fe(II) is tetrahedral with two coordinating carbenes and two chlorine atoms. (Figure S1) The C-Fe distances are 2.1464(17) and 2.1529(17) Å which is close to the corresponding bond lengths in the earlier reported $(NHC)_2FeCl_2$.[S6] C–Fe–C bond angle is 115.36(6) ° and Cl–Fe–Cl angle is 112.92(2) °. **1** in solid state is stable in air for certain hours but the decomposition is faster in solutions when exposed to air.

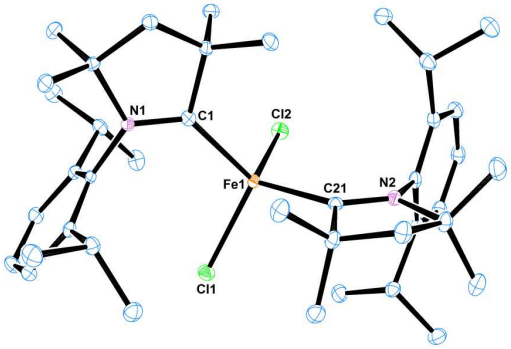

Figure S1. Molecular structure of **1**. Hydrogen atoms are omitted for clarity. Anisotropic displacement parameters are depicted at the 50% probability level. Selected bond lengths [Å] and angles [°] Fe1–C1, 2.1464(17); Fe1–C21, 2.1529(17); Fe1–Cl1, 2.2873(5); Fe1–Cl2, 2.2745(7); C1–N1, 1.317(2); C21–N2, 1.317(2); C1–Fe1–Cl1, 107.66(5); C1–Fe1–Cl2, 104.58(5); C21–Fe1–Cl1, 107.37(5); C21–Fe1–Cl2, 109.08(5).

Molecular structure of 3

The molecular structure of $[(cAAC)_2Fe]^+[B(C_6F_5)_4]^-$ is given in figure S2. While the Fe atom adopts a linear coordination, the geometry around boron atom is tetrahedral. The Fe1····B1 distance is 8.885 Å.

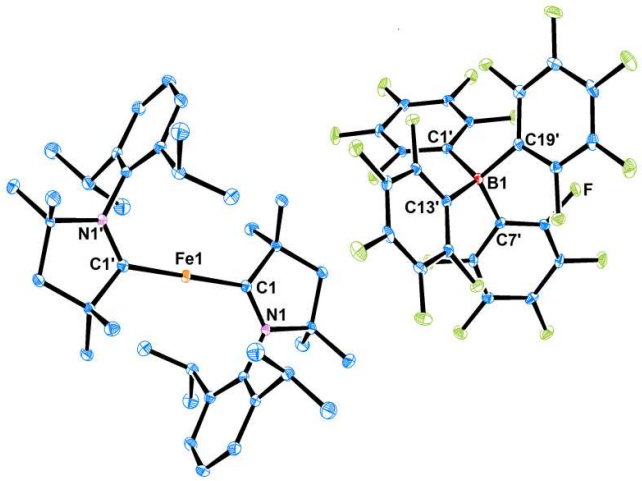

Figure S2. Molecular structure of **3**. Hydrogen atoms are omitted for clarity. Anisotropic displacement parameters are depicted at the 50% probability level. Selected bond lengths [Å] and angles [°] Fe1–C1 / Fe2–C1A, 1.999(2)/ 2.008(2); C1–N1 / C1A–N1A, 1.315(2)/1.313(2); C1–Fe1–C1', 180.

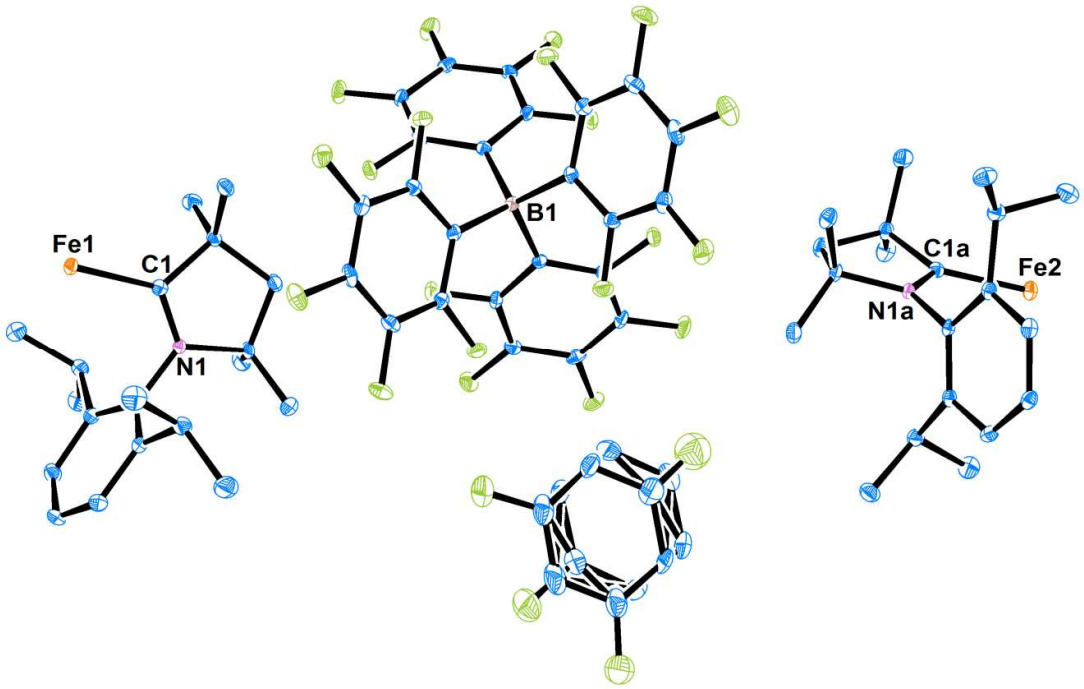

Figure S3. The asymmetric unit of **3**. Anisotropic displacement parameters are depicted at the 50% probability level. Hydrogen atoms are omitted for clarity

S2. Mössbauer Spectroscopy

Mössbauer spectra were recorded with a ^{57}Co source in a Rh matrix using an alternating constant acceleration *Wissel* mössbauer spectrometer operated in the transmission mode and equipped with a *Janis* closed-cycle helium cryostat. Isomer shifts are given relative

to iron metal at ambient temperature. Simulation of the experimental data was performed with the *Mfit* program.[S7]

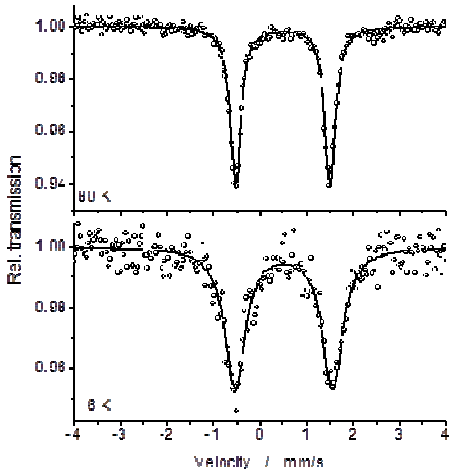

Figure S4. Comparison of the Mössbauer spectra of **2** at 80 K (top) and 6 K (bottom).

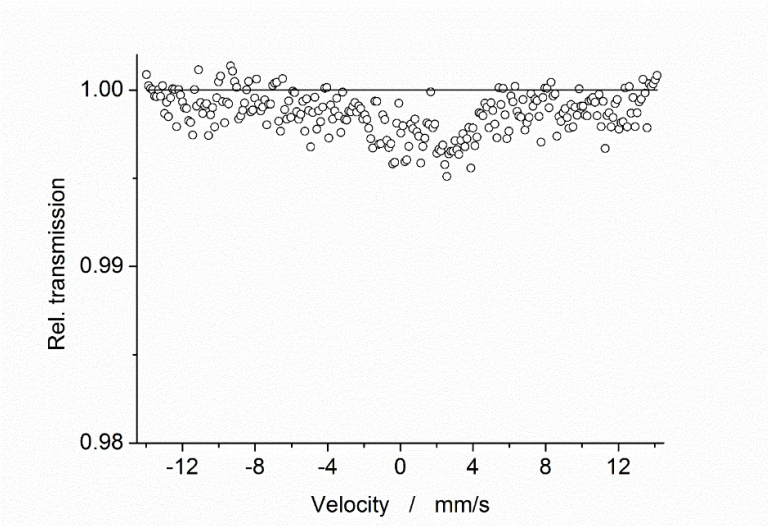

Figure S5. Mössbauer spectrum of **3** at 6 K. The solid line shows 100 % transmission level. Deviation from this line clearly indicates that the Mössbauer signal doesn't disappear but becomes broader and probably splits in six lines due to slow paramagnetic relaxation.

S3. Magnetic measurements

Temperature-dependent magnetic susceptibility measurements were carried out with a *Quantum-Design* MPMS-XL-5 SQUID magnetometer equipped with a 5 Tesla magnet in the range from 2 to 295 K for **2** and from 2 to 215 K for **3** at a magnetic field of 0.5 T. The powdered sample was contained in a gel bucket and fixed in a non-magnetic sample holder. Each raw data file for the measured magnetic moment was corrected for the diamagnetic contribution of the sample holder and the gel bucket. The molar susceptibility data were

corrected for the diamagnetic contribution. Temperature-independent paramagnetism (*TIP*) was included according to $\chi_{calc} = \chi + TIP$. Before simulation, the experimental data were corrected for *TIP*: *TIP* = $770 \cdot 10^{-6}$ cm^3mol^{-1} for **2** and $1290 \cdot 10^{-6}$ cm^3mol^{-1} for **3** ($1000 \cdot 10^{-6}$ cm^3mol^{-1} (fixed) for VTVH measurement of **3**). Diamagnetic impurities of 5 % were included for simulation of the VTVH data of **2** to get better agreement with experimental values.

Experimental data for **2** and **3** were modelled using a fitting procedure to the appropriate Heisenberg-Dirac-van Vleck spin Hamiltonian for one iron $S = 3/2$ with Zeemann splitting and zero-field splitting.

$$\hat{H} = g\mu_B \vec{B}\vec{S} + D\left[\hat{S}_z^2 - \frac{1}{3}S(S+1) + E/D(\hat{S}_x^2 - \hat{S}_y^2)\right] \quad \text{.....(1)}$$

The ratio E/D was fixed to 0.01 for **2** and to zero for **3**. Simulation of the experimental magnetic data was performed with the *julX* program.[S8]

S 4. EPR spectroscopy

High-frequency EPR measurements were conducted at the Florida State University National High Magnetic Field Laboratory (FSU-NHMFL) in Tallahassee, FL. The HF-EPR operates in transmission mode and employs cylindrical waveguides, as described elsewhere.[S9] Microwave detection was performed with a low-noise, fast-response InSb hot-electron bolometer (QMC Ltd.). The magnetic field was calibrated using a DPPH standard (g=2.0036). X-band (9.4 GHz) measurements were performed using a Bruker Elxsys-500 spectrometer.

HF-EPR of randomly oriented polycrystalline samples was measured to obtain precise information on the spin state and the magnetic parameters (zero-field splitting, the D and E parameters, see the definition below) of both compounds. EPR was measured at 336 and 240 GHz between 0 and 12.5 T in the range of 3-290 K. The EPR spectra were analyzed using the spin Hamiltonian in Eq. (2).[S10]

$$\hat{H} = \beta \boldsymbol{H} \cdot \boldsymbol{g} \cdot \hat{\boldsymbol{S}} + D\left(\hat{S}_z^{\,2} - \hat{\boldsymbol{S}}^2/3\right) + E\left(\hat{S}_x^{\,2} - \hat{S}_y^{\,2}\right) \quad \cdots\cdots\cdots (2)$$

In this Hamiltonian, $\boldsymbol{g}$ is the Zeeman tensor, D and E are the axial and rhombic second order zero-field splitting parameters, and the other terms pertain their usual meaning.[S10,S11] The hyperfine interaction is omitted because the magnetic isotope of Fe (i.e. ^{57}Fe, with $I = {}^1/_2$) has

rather small (~ 2.1 %) natural abundance, thus each peak of the hyperfine doublet would be ~ 1% of the main peaks, and thus would be hardly detectable, as was the case here. A locally developed computer program was utilized to diagonalize the Hamiltonian matrix of Eq. (2), and obtain an energy-level diagram as a function of the Zeeman field.[S12]

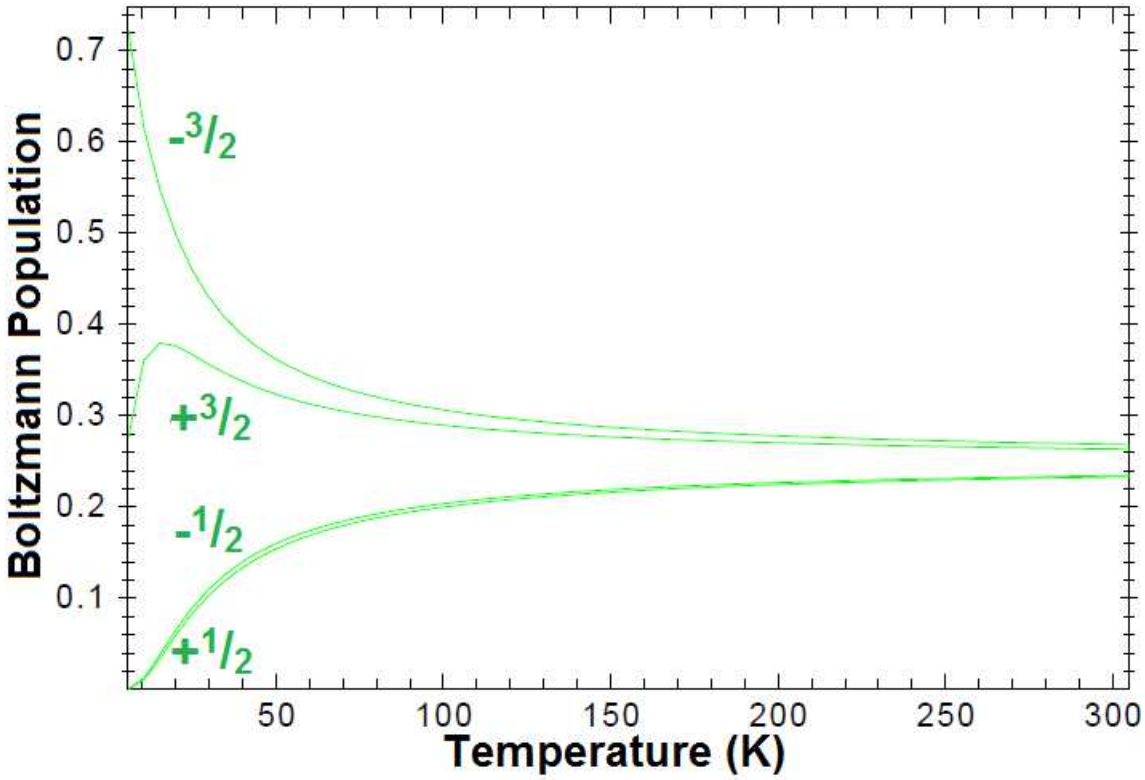

Figure S6. The Boltzmann population for **3** is calculated using $S = {}^{3}/_{2}$, D = -13.6 cm^{-1}, and isotropic g = 2.45. The green numbers represent the M_s quantum numbers in the high-field limit. At low temperatures (< 20 K) it is seen that the ± 3/2 states are the most populated. Due to the fast spin-lattice relaxation of Fe(I) it is necessary to measure EPR at low temperatures, thus the only EPR transition would be strongly forbidden (ΔMs = 3), and is not expected to be observed, as was seen here.

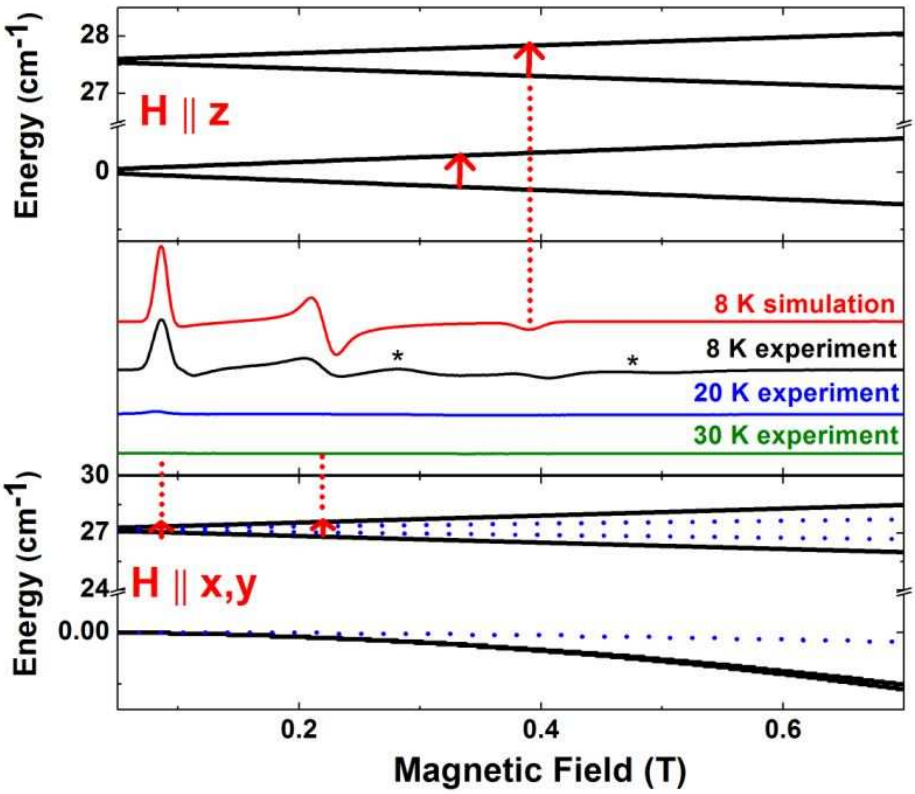

Figure S7. 9.4 GHz experimental and simulated EPR spectrum of compound **3**. The top portion shows the energy level diagram for the Zeeman field parallel to the principal symmetry direction, z. The bottom portion shows the energy perpendicular to this direction (black solid trace is the x direction, blue dotted trace is the y direction). Red arrows mark the EPR transition assignment. No spectra were observed above 20 K likely due to fast spin-lattice relaxation. The experimental spectra yield an excellent fit using $S = 3/2$, $g_x = 3.7$, $g_y = 1.7$, $g_z = 1.7$, and $D = -13.6$ cm^{-1}. The stars in the figure indicate two small features whose origin is unknown at this time.

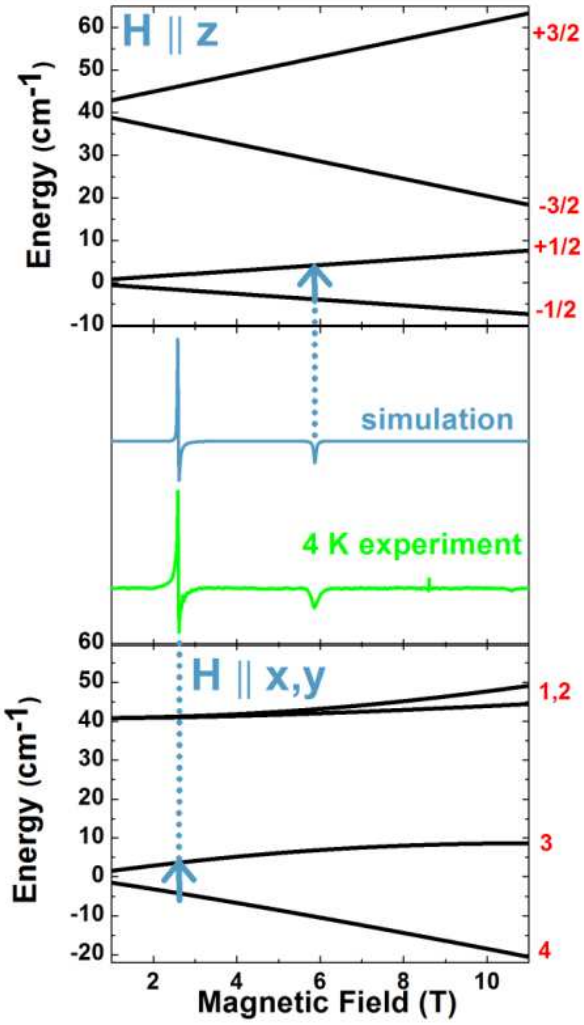

Figure S8. 240 GHz experimental and simulated EPR spectrum of compound **2** at 4 K. The top and bottom portions show the energy level diagram for the Zeeman field H parallel (top) and perpendicular (bottom) to the principal symmetry axes. The red numbers in the top figure represent the M_s quantum numbers in the high-field limit. In the bottom figure; however, they are just a label for an energy level since the field strength was not enough to be in the 'high-field' limit. Blue arrows mark the EPR transition assignment. The experimental spectrum yields an excellent fit using $S = 3/2$, $g_x = 3.33$, $g_y = 3.33$, $g_z = 2.91$, and $D = 20.4$ cm^{-1}. Above 8 T two small features are seen, which are attributed to a paramagnetic impurity.

S5. Theoretical Calculations

Ab initio calculations were performed in order to get an insight into the low-lying electronic structure. All calculations were performed with MOLCAS 7.8[S13] and were of CASSCF/CASPT2/SO-RASSI type.

Computational details:

In order to reach computational feasibility, we have investigated smaller models of **1**, **2** and **3**, in which bulky alkyl ligands were removed, while the remaining bonds were saturated by H. Since the alkyl ligands do not participate in the electron transfer processes (in contrast to conjugated ligands or organic radicals), the calculated structural models are expected to be reliable for the purposes of the determination of the electronic configuration around the metal site. Figure S9 shows the structure of the computed models of **1**, **2** and **3**.

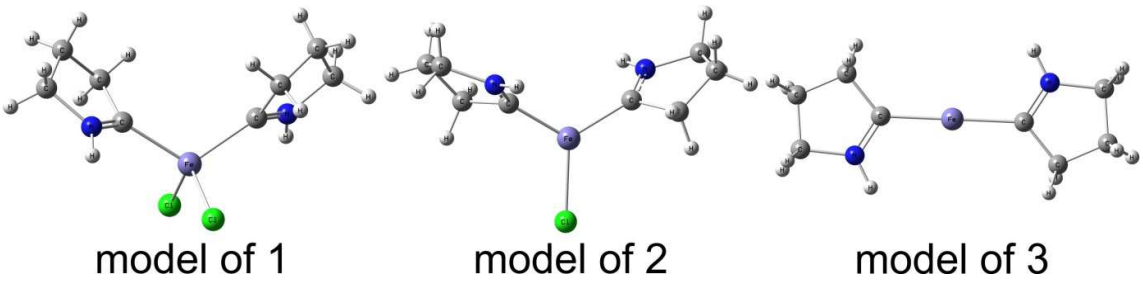

Figure S9. The structure of the computational models employed in the *ab initio* study.

Each atom was described by the all-electron relativistic ANO-RCC basis functions. Basis sets of single-zeta (SZ), double-zeta plus polarization (DZP) and triply zeta plus polarization (TZP) were employed.

The active space of the CASSCF method was investigated extensively, in order to understand the nature of important interactions. In the first step, the minimal active space was employed. Further, it was increased gradually, by adding (bonding and antibonding) orbitals of the

bonding carbon atoms ($2p_{xyz}$-C), 4s-Fe, etc. Notation CAS(*n*,*m*) refers to a CASSCF calculation involving all possible configurations arising from distributing *n* electrons among *m* orbitals.

The following tables give the obtained energies and the *g* tensors of the ground manifolds.

Results of the ab initio calculations for compound 1.

For **1**, the multiconfigurational *ab initio* calculations show that iron has a clear $3d^6$ character, i.e., it is Fe(II). The addition of ligand bonding/antibonding orbitals of the bonded carbon atoms into the active space of the CASSCF method does not change this picture. All spin density is localized on Fe site, in the 3d shell. The low-lying electronic structure is dominated by the relatively weak ligand field splitting of the ground ^5D manifold (≈5500 cm^{-1} or ≈0.68 eV). The lowest spin triplet and spin singlet states lie much higher in energy (2.0 eV and 3.2 eV, respectively). The splitting of the ground ^5D manifold is rather interesting as no clear terms *E* and T_2 can be recognized, as one would expect for a d^6 in tetrahedral environment. The reason for this unusual splitting pattern is the strong deviation of the ligand field on the Fe ion from tetrahedral symmetry, arising from the different effect of the carbon and chlorine atoms. Thus the separation between the ground and first excited spin quintet states is ≈1400 cm^{-1} (0.17 eV), nearly three times larger than the spin-orbit coupling constant for Fe(II) ion.[S14] As a result, the effect of the spin-orbit coupling is relatively weak. The combined effect of low-symmetry environment surrounding the metal site and the spin-orbit coupling on Fe(II) leads to relatively small zero-field splitting of the ground spin quintet. The calculated parameters of Zeeman Hamiltonian (in terms of pseudospin S=2) are g_X=2.033 ; g_Y= 2.085, g_Z= 2.171, and of the second-order ZFS Hamiltonian are: *D*= -5.85 cm^{-1}; *E*= 1.27 cm^{-1}.

Table S2. CASSCF energies of the low-lying orbital spin quintet states and energies of the resulting spin-orbital states in various computational models, main values of the *g* tensor of the ground pseudospin *S*=2, and the corresponding second-order zero-field splitting parameters (*D* and *E*).

CASSCF energies of the low-lying spin quintets (S=5). All triplets and singlets are much higher in energy.							
SZ	SZ	SZ	SZ	SZ	DZP	DZP	TZP
CAS (6,5)	CAS (6,7)	CAS (10,9)	CAS (14,12)	CAS (16,14)	CAS (6,5)	CAS (6,10)	CAS (6,5)
0	0	0	0	0	0	0	0
1060	1221	927	959	1056	1348	1759	1414
2972	2935	2844	2868	2949	3140	3491	3229
4784	4946	4688	4716	4755	5015	5588	4954
5394	5429	5241	5299	5372	5585	6201	5622
CASSCF / RASSI-SO energies of the low-lying spin-orbit states							
0.0	0.0	0.0	0.0	0.0	0.0	0.0	0.0
1.6	1.6	1.8	1.2	0.9	0.8	0.4	0.8
17.5	16.9	17.4	14.3	14.6	21.0	17.2	20.1
29.2	28.2	30.1	23.5	22.3	29.4	22.1	28.1
31.9	30.9	32.6	25.9	25.0	34.0	26.4	32.5
1063.9	1222.7	933.1	964.2	1058.3	1347.4	1754.4	1413.2
1069.3	1228.3	937.9	967.8	1062.0	1353.7	1759.3	1419.2
1072.4	1231.1	941.5	971.3	1066.1	1357.7	1764.1	1423.2
1091.8	1251.0	959.8	985.6	1080.9	1380.4	1783.1	1445.2
1092.3	1251.4	960.4	986.0	1081.5	1381.0	1783.6	1445.8
3002.3	2966.4	2878.7	2899.8	2978.7	3167.6	3509.0	3251.8
3006.6	2971.6	2881.8	2901.0	2980.5	3173.8	3514.9	3258.5
3015.4	2978.5	2893.0	2917.4	2994.9	3180.6	3519.4	3264.9
3035.9	3000.2	2910.8	2929.9	3009.2	3205.7	3541.2	3291.2
3036.6	3000.8	2911.9	2932.4	3011.0	3206.4	3541.7	3292.0
4839.7	4998.8	4741.5	4768.7	4808.8	5072.2	5634.5	5014.5
4842.8	5001.5	4744.4	4771.6	4811.0	5074.0	5635.6	5016.0
4846.0	5005.0	4749.7	4775.6	4817.0	5082.4	5640.1	5023.7
4858.4	5016.6	4762.8	4787.5	4827.5	5093.6	5646.5	5033.5
4858.9	5016.9	4763.4	4788.1	4828.1	5095.1	5647.2	5034.9
5473.6	5507.8	5324.3	5376.2	5445.2	5670.5	6261.8	5702.5
5474.8	5508.7	5324.8	5379.0	5449.6	5671.6	6262.0	5703.2
5477.1	5512.2	5330.9	5382.5	5450.4	5675.5	6267.1	5709.8
5481.7	5516.6	5334.2	5392.8	5463.4	5680.8	6269.3	5714.0
5482.1	5517.3	5335.6	5393.4	5463.8	5681.1	6270.6	5715.5
Calculated main values of the *g* tensor (g_X, g_Y, g_Z) of the ground manifold (pseudospin *S*=2)							
2.033	2.033	2.030	2.029	2.033	2.037	2.036	2.038
2.089	2.086	2.094	2.093	2.084	2.076	2.057	2.075
2.167	2.160	2.174	2.174	2.171	2.175	2.138	2.171
Calculated zero-field splitting (ZFS) parameters: the axial *D* and rhombic *E* parameters of the ground manifold (pseudospin *S*=2)							
D= -7.25 *E*= 1.93	*D*= -7.02 *E*= 1.87	*D*= -7.32 *E*= 2.09	*D*= -5.89 *E*= 1.53	*D*= -5.85 *E*= 1.27	*D*= -8.14 *E*= 1.38	*D*= -6.43 *E*= 0.81	*D*=-7.79 *E*=1.32

Table S3. CASSCF/CASPT2 energies of the low-lying orbital spin quintet states and energies of the resulting spin-orbital states in various computational models, main values of the *g* tensor of the ground pseudospin *S*=2, and the corresponding second-order zero-field splitting parameters (*D* and *E*).

CASSCF /CASPT2 energies of the low-lying spin quintets (S=5).					
SZ	SZ	SZ	SZ	DZP	DZP
CAS (6,5)	CAS (6,7)	CAS (10,9)	CAS (14,12)	CAS (6,5)	CAS (6,10)
0	0	0.0	0	0	0
1354	1433	1302.0	1328	1847	1976
3381	3374	3330.1	3352	3980	4097
4956	5073	4946.5	4876	6068	5999
5871	5851	5774.2	5753	6917	6992
CASSCF/CASPT2/RASSI-SO energies of the low-lying spin-orbit states					
0.0	0.0	0.0	0.0	0.0	0.0
1.6	1.4	1.8	1.0	0.5	0.4
16.3	16.0	15.5	11.8	18.7	16.7
27.4	26.3	27.3	19.6	24.7	21.1
30.0	29.0	29.6	21.6	29.2	25.3
1357.3	1434.4	1304.3	1329.2	1845.7	1973.6
1362.2	1439.5	1308.9	1332.4	1851.6	1978.8
1365.7	1442.5	1312.6	1335.9	1854.7	1981.8
1383.9	1461.0	1330.1	1349.1	1875.1	2000.1
1384.3	1461.4	1330.6	1349.5	1875.5	2000.4
3400.4	3393.1	3351.0	3370.5	3993.7	4106.4
3406.9	3400.0	3356.8	3373.9	4000.2	4111.8
3413.0	3405.0	3363.6	3385.6	4006.4	4117.8
3438.2	3430.4	3387.2	3404.8	4031.6	4139.3
3438.8	3431.0	3387.9	3405.8	4032.1	4139.8
5015.9	5131.0	5004.6	4933.3	6121.1	6044.7
5017.6	5132.6	5006.7	4933.5	6122.1	6045.7
5022.3	5136.4	5010.6	4944.2	6128.2	6050.0
5031.1	5144.4	5020.3	4948.1	6135.1	6055.7
5031.6	5144.7	5020.6	4950.7	6136.1	6056.3
5940.7	5919.4	5845.5	5818.0	6981.2	7043.1
5940.9	5919.6	5846.2	5819.3	6981.3	7043.3
5947.6	5926.8	5851.3	5829.4	6988.6	7049.7
5949.7	5928.9	5855.6	5837.3	6990.9	7052.3
5951.5	5930.8	5856.6	5839.3	6992.7	7053.8
Calculated main values of the *g* tensor (g_X, g_Y, g_Z) of the ground manifold (pseudospin *S*=2)					
2.035	2.037	2.031	2.033	2.039	2.035
2.082	2.079	2.086	2.083	2.060	2.051
2.150	2.144	2.151	2.155	2.138	2.122
Calculated zero-field splitting (ZFS) parameters: the axial *D* and rhombic *E* parameters of the ground manifold (pseudospin *S*=2)					
D=-6.78	*D*=-6.61	*D*=-6.57	*D*=-4.93	*D*=-7.08	*D*=-6.19
E=1.84	*E*=1.71	*E*=1.96	*E*=1.29	*E*=0.98	*E*=0.73

Results of the ab initio calculations for compound 2.

Table S4. CASSCF energies of the low-lying orbital spin quartet states and energies of the resulting spin-orbital states in various computational models, main values of the *g* tensor of the ground pseudospin *S*=3/2, and the corresponding second-order zero-field splitting parameters (*D* and *E*).

CASSCF energies of the low-lying spin quintets (S=3/2). All doublets and sextets are much higher in energy.								
SZ	SZ	SZ	SZ	SZ	DZP	DZP	TZP	TZP
CAS (7,5)	CAS (9,9)	CAS (13,11)	CAS (21,12)	CAS (27,15)	CAS (7,5)	CAS (7,10)	CAS (7,5)	CAS (7,10)
0	0	0	0	0	0	0	0	0
1336	644	965	1377	1377	607	1715	630	1707
1395	1259	1340	1398	1398	808	1755	809	1803
5714	6149	6512	5859	5859	3773	6433	3836	6419
7847	9480	8577	7971	7970	6291	8804	6359	8838
8133	10592	9820	8274	8273	6530	9066	6619	9042
9195	11175	10387	9384	9383	7519	10644	7617	10707
CASSCF / RASSI-SO energies of the low-lying spin-orbit states								
0.0	0.0	0.0	0.0	0.0	0.0	0.0	0.0	0.0
0.0	0.0	0.0	0.0	0.0	0.0	0.0	0.0	0.0
52.5	76.5	57.5	54.5	54.5	74.6	33.3	73.9	33.9
52.5	76.5	57.5	54.5	54.5	74.6	33.3	73.9	33.9
1264.7	736.1	991.4	1283.3	1283.5	679.3	1603.7	693.9	1620.0
1264.7	736.1	991.4	1283.3	1283.5	679.3	1603.7	693.9	1620.0
1472.5	880.3	1129.3	1491.9	1492.1	881.2	1777.0	898.1	1785.6
1472.5	880.3	1129.3	1491.9	1492.1	881.2	1777.0	898.1	1785.6
1604.5	1447.7	1502.3	1620.2	1620.4	1040.5	1911.6	1043.2	1945.3
1604.5	1447.7	1502.3	1620.2	1620.4	1040.5	1911.6	1043.2	1945.3
1758.9	1523.7	1606.7	1792.5	1792.7	1208.5	2040.9	1214.0	2066.2
1758.9	1523.7	1606.7	1792.5	1792.7	1208.5	2040.9	1214.0	2066.2
5795.0	6284.4	6619.5	5943.2	5943.4	3945.5	6479.3	4006.1	6465.2
5795.0	6284.4	6619.5	5943.2	5943.4	3945.5	6479.3	4006.1	6465.2
5832.6	6300.5	6626.1	5976.3	5976.6	3970.3	6504.6	4031.4	6491.6
5832.6	6300.5	6626.1	5976.3	5976.6	3970.3	6504.6	4031.4	6491.6
7811.2	9540.6	8619.7	7938.5	7937.5	6392.3	8772.9	6460.4	8801.6
7811.2	9540.6	8619.7	7938.5	7937.5	6392.3	8772.9	6460.4	8801.6
7941.5	9590.4	8660.8	8074.9	8073.8	6445.6	8864.1	6515.0	8898.2
7941.5	9590.4	8660.8	8074.9	8073.8	6445.6	8864.1	6515.0	8898.2
8251.5	10701.4	9887.8	8402.6	8401.6	6667.8	9147.3	6754.6	9124.3
8251.5	10701.4	9887.8	8402.6	8401.6	6667.8	9147.3	6754.6	9124.3
8378.1	10794.2	9980.3	8520.3	8519.2	6793.0	9225.6	6876.7	9211.5
8378.1	10794.2	9980.3	8520.3	8519.2	6793.0	9225.6	6876.7	9211.5
9395.9	11358.9	10533.3	9584.7	9583.7	7790.6	10761.2	7886.2	10824.6
9395.9	11358.9	10533.3	9584.7	9583.7	7790.6	10761.2	7886.2	10824.6
9471.3	11423.1	10604.4	9658.0	9657.0	7869.1	10797.3	7963.5	10859.3
9471.3	11423.1	10604.4	9658.0	9657.0	7869.1	10797.3	7963.5	10859.3
Calculated main values of the *g* tensor (g_X, g_Y, g_Z) of the ground manifold (pseudospin *S*=3/2)								
2.601	2.770	2.574	2.583	2.583	2.866	2.406	2.846	2.410
2.500	2.371	2.406	2.499	2.499	2.747	2.370	2.752	2.364
2.047	1.946	1.973	2.048	2.048	1.980	2.036	1.981	2.035
Calculated zero-field splitting (ZFS) parameters: the axial *D* and rhombic *E* parameters of the ground manifold (pseudospin *S*=3/2)								
D=25.9	*D*=34.9	*D*=26.8	*D*=27.1	*D*=27.1	*D*= 36.4	*D*= 16.6	*D*= 36.3	*D*= 16.8
E=-2.3	*E*=-9.0	*E*=-5.9	*E*=-1.9	*E*=-1.9	*E*= -4.6	*E*= -0.9	*E*= -3.8	*E*= -1.3

Table S5. CASSCF/CASPT2 energies of the low-lying orbital spin quartet states and energies of the resulting spin-orbital states in various computational models, main values of the *g* tensor of the ground pseudospin *S*=3/2, and the corresponding second-order zero-field splitting parameters (*D* and *E*).

CASSCF /CASPT2 energies of the low-lying spin quintets (S=3/2).							
SZ	SZ	SZ	SZ	SZ	DZP	DZP	TZP
CAS (7,5)	CAS (9,9)	CAS (13,11)	CAS (21,12)	CAS (27,15)	CAS (7,5)	CAS (7,10)	CAS (7,5)
0	0	0	0	0	0	0	0
2302	688	1512	1696	1644	2113	1534	1787
2674	941	1759	2268	2226	2579	1825	2357
8467	6767	7171	8548	8526	7994	6826	7762
12533	8577	8037	12825	12882	10757	9463	10468
13807	9775	9936	14052	14056	10901	9682	10577
15678	10265	10379	15638	15688	14888	12208	14875
CASSCF/CASPT2/RASSI-SO energies of the low-lying spin-orbit states							
0.0	0.0	0.0	0.0	0.0	0.0	0.0	0
0.0	0.0	0.0	0.0	0.0	0.0	0.0	0
27.0	73.4	43.0	40.7	41.7	24.0	32.5	27
27.0	73.4	43.0	40.7	41.7	24.0	32.5	27
2227.7	722.7	1472.4	1682.9	1633.6	2056.3	1502.2	1744
2227.7	722.7	1472.4	1682.9	1633.6	2056.3	1502.2	1744
2374.8	912.9	1615.6	1805.8	1756.8	2189.8	1636.3	1877
2374.8	912.9	1615.6	1805.8	1756.8	2189.8	1636.3	1877
2783.7	1157.5	1891.7	2392.2	2351.3	2666.0	1937.9	2447
2783.7	1157.5	1891.7	2392.2	2351.3	2666.0	1937.9	2447
2889.0	1304.5	2011.4	2486.1	2445.0	2765.6	2033.1	2544
2889.0	1304.5	2011.4	2486.1	2445.0	2765.6	2033.1	2544
8507.6	6908.3	7228.2	8627.9	8607.6	8019.6	6867.1	7789
8507.6	6908.3	7228.2	8627.9	8607.6	8019.6	6867.1	7789
8531.1	6919.3	7251.2	8638.4	8617.8	8042.6	6896.2	7813
8531.1	6919.3	7251.2	8638.4	8617.8	8042.6	6896.2	7813
12247.3	8659.6	8081.3	12795.4	12850.1	9954.4	9442.9	8488
12247.3	8659.6	8081.3	12795.4	12850.1	9954.4	9442.9	8488
12538.1	8699.6	8115.3	12894.8	12952.9	10533.3	9531.3	9395
12538.1	8699.6	8115.3	12894.8	12952.9	10533.3	9531.3	9395
12838.3	9874.1	9962.8	14149.7	14156.7	10741.6	9755.8	10314
12838.3	9874.1	9962.8	14149.7	14156.7	10741.6	9755.8	10314
13817.5	9970.1	10043.0	14210.2	14222.2	10922.5	9842.1	10491
13817.5	9970.1	10043.0	14210.2	14222.2	10922.5	9842.1	10491
13900.1	10452.1	10492.3	15745.3	15795.9	11045.4	12288.9	10686
13900.1	10452.1	10492.3	15745.3	15795.9	11045.4	12288.9	10686
14548.2	10534.0	10563.7	15775.2	15824.2	11269.8	12301.3	10867
14548.2	10534.0	10563.7	15775.2	15824.2	11269.8	12301.3	10867
Calculated main values of the *g* tensor (g_X, g_Y, g_Z) of the ground manifold (pseudospin *S*=3/2)							
2.348	2.493	2.406	2.448	2.458	2.317	2.394	2.356
2.257	2.334	2.341	2.290	2.294	2.279	2.370	2.286
2.045	1.983	1.990	2.040	2.039	2.046	2.031	2.043
Calculated zero-field splitting (ZFS) parameters: the axial *D* and rhombic *E* parameters of the ground manifold (pseudospin *S*=2)							
D=13.0 *E*=-2.1	*D*=23.01 *E*=-4.67	*D*=21.1 *E*=-2.4	*D*=18.8 *E*=-4.4	*D*= 19.2 *E*= -4.6	*D*= 11.8 *E*= -1.3	*D*= 16.2 *E*=-1.0	*D*= 13.2 *E*= -2.4

Results of the ab initio calculations for compound 3.

Table S6. CASSCF energies of the low-lying orbital spin quartet states and energies of the resulting spin-orbital states in various computational models, main values of the *g* tensor of the ground pseudospin *S*=1/2.

Molecule 1 (Fe-C bond 2.00814 Å)

CASSCF energies of the low-lying spin quintets (S=3/2). All doublets and sextets are much higher in energy.								
SZ	SZ	SZ	SZ		DZP	DZP	TZP	TZP
CAS (7,5)	CAS (7,7)	CAS (11,9)	CAS (15,13)		CAS (7,5)	CAS (7,10)	CAS (7,5)	CAS (7,10)
0	0	0	0		0	0	0	0
305	241	727	622		526	1062	571	935
380	290	775	673		598	1170	645	1030
979	2174	2150	2195		1022	1440	981	1312
1739	4439	3687	3922		1074	1747	1040	1657
3098	5747	4980	5163		1818	3428	1851	3082
3222	6088	5562	5695		2008	3674	2059	3419
CASSCF / RASSI-SO energies of the low-lying spin-orbit states								
0.0	0.0	0.0	0.0		0.0	0.0	0.0	0.0
0.0	0.0	0.0	0.0		0.0	0.0	0.0	0.0
81.8	68.9	30.4	28.7		63.0	45.0	43.5	40.4
81.8	68.9	30.4	28.7		63.0	45.0	43.5	40.4
241.5	119.6	479.5	383.6		403.0	861.6	425.2	732.5
241.5	119.6	479.5	383.6		403.0	861.6	425.2	732.5
570.8	494.6	775.0	687.5		761.5	1057.0	753.6	944.5
570.8	494.6	775.0	687.5		761.5	1057.0	753.6	944.5
673.7	645.9	986.9	898.3		842.6	1188.2	840.9	1092.8
673.7	645.9	986.9	898.3		842.6	1188.2	840.9	1092.8
1010.6	918.4	1266.7	1174.9		1008.8	1497.6	1003.8	1376.0
1010.6	918.4	1266.7	1174.9		1008.8	1497.6	1003.8	1376.0
1238.3	2392.8	2260.1	2312.4		1094.8	1546.8	1087.1	1432.1
1238.3	2392.8	2260.1	2312.4		1094.8	1546.8	1087.1	1432.1
1382.8	2425.9	2301.8	2348.8		1215.5	1716.7	1205.3	1604.3
1382.8	2425.9	2301.8	2348.8		1215.5	1716.7	1205.3	1604.3
2102.5	4682.9	3835.6	4071.2		1463.2	1958.3	1427.4	1870.5
2102.5	4682.9	3835.6	4071.2		1463.2	1958.3	1427.4	1870.5
2237.2	4713.7	3880.0	4121.2		1698.6	2138.9	1655.7	2035.3
2237.2	4713.7	3880.0	4121.2		1698.6	2138.9	1655.7	2035.3
2910.3	5627.3	4863.8	5049.0		1831.1	3228.0	1852.3	2958.4
2910.3	5627.3	4863.8	5049.0		1831.1	3228.0	1852.3	2958.4
3286.4	5913.9	5074.6	5259.0		2110.2	3514.0	2131.6	3209.5
3286.4	5913.9	5074.6	5259.0		2110.2	3514.0	2131.6	3209.5
3672.1	6383.3	5729.7	5868.4		2447.0	3905.6	2475.9	3655.5
3672.1	6383.3	5729.7	5868.4		2447.0	3905.6	2475.9	3655.5
4014.5	6657.4	5935.0	6081.7		2678.2	4167.9	2698.3	3883.3
4014.5	6657.4	5935.0	6081.7		2678.2	4167.9	2698.3	3883.3
Calculated main values of the *g* tensor (g_X, g_Y, g_Z) of the ground manifold (pseudospin *S*=1/2)								
0.569	0.104	1.962	1.449		0.811	1.855	0.819	2.072
0.833	0.141	3.583	2.198		0.971	3.155	1.154	3.960
9.492	9.269	6.133	7.136		9.260	6.793	8.893	6.308

Molecule 2 (Fe-C bond 1.99872 Å)

CASSCF energies of the low-lying spin quintets (S=3/2). All doublets and sextets are much higher in energy.								
SZ	SZ	SZ	SZ		DZP	DZP		
CAS (7,5)	CAS (7,7)	CAS (11,9)	CAS (15,13)		CAS (7,5)	CAS (7,10)		
0	0	0	0		0	0		
439	489	992	908		530	1290		
475	513	1021	938		632	1378		
983	2279	2217	2276		1158	1507		
1734	4424	3658	3881		1226	1759		
3166	5687	4901	5056		1927	3492		
3321	6129	5635	5751		2163	3820		
CASSCF / RASSI-SO energies of the low-lying spin-orbit states								
0.0	0.0	0.0	0.0		0.0	0.0		
0.0	0.0	0.0	0.0		0.0	0.0		
23.1	24.5	26.9	18.8		63.8	47.1		
23.1	24.5	26.9	18.8		63.8	47.1		
273.8	248.7	707.8	622.9		413.0	1073.8		
273.8	248.7	707.8	622.9		413.0	1073.8		
564.4	580.7	986.6	907.3		781.1	1199.1		
564.4	580.7	986.6	907.3		781.1	1199.1		
709.9	782.3	1209.3	1132.3		918.8	1344.0		
709.9	782.3	1209.3	1132.3		918.8	1344.0		
1046.2	1056.5	1493.2	1412.4		1083.0	1591.9		
1046.2	1056.5	1493.2	1412.4		1083.0	1591.9		
1202.7	2416.6	2311.0	2366.6		1154.9	1687.4		
1202.7	2416.6	2311.0	2366.6		1154.9	1687.4		
1351.4	2447.3	2350.6	2402.1		1301.4	1872.9		
1351.4	2447.3	2350.6	2402.1		1301.4	1872.9		
2036.2	4587.0	3788.8	4004.2		1571.6	1971.8		
2036.2	4587.0	3788.8	4004.2		1571.6	1971.8		
2169.6	4618.4	3833.4	4054.1		1832.1	2169.2		
2169.6	4618.4	3833.4	4054.1		1832.1	2169.2		
2935.0	5525.6	4808.3	4961.2		1943.5	3321.0		
2935.0	5525.6	4808.3	4961.2		1943.5	3321.0		
3303.7	5785.4	4984.2	5133.3		2217.7	3584.6		
3303.7	5785.4	4984.2	5133.3		2217.7	3584.6		
3698.6	6328.8	5774.0	5887.0		2580.0	4030.2		
3698.6	6328.8	5774.0	5887.0		2580.0	4030.2		
4034.6	6576.6	5946.6	6063.9		2803.3	4271.6		
4034.6	6576.6	5946.6	6063.9		2803.3	4271.6		
Calculated main values of the g tensor (g_X, g_Y, g_Z) of the ground manifold (pseudospin S=1/2)								
1.521	1.722	5.287	4.853		0.607	1.778		
2.237	2.810	4.200	4.680		0.717	2.964		
8.005	6.884	2.127	2.150		9.257	6.835		

Table S7. CASSCF/CASPT2 energies of the low-lying orbital spin quartet states and energies of the resulting spin-orbital states in various computational models, main values of the *g* tensor of the ground pseudospin *S*=1/2.

Molecule 1 (Fe-C bond 2.00814 Å)

CASSCF /CASPT2 energies of the low-lying spin quintets (S=3/2).								
SZ	SZ	SZ	SZ		DZP	DZP	TZP	TZP
CAS (7,5)	CAS (7,7)	CAS (11,9)	CAS (15,13)		CAS (7,5)	CAS (7,10)	CAS (7,5)	CAS (7,10)
0	0	0	0		0	0	0	0
51	645	1017	962		1934	1429	2104	1257
181	678	1074	1014		2298	1672	2286	1579
1641	2228	2398	2485		2338	1819	2794	1699
5249	4824	4808	4764		4928	2180	4966	1868
6716	5924	5876	5787		6333	3904	6218	3258
6864	6253	6364	6293		7025	4400	7024	3991
CASSCF/CASPT2/RASSI-SO energies of the low-lying spin-orbit states								
0.0	0.0	0.0	0.0		0.0	0.0	0.0	0.0
0.0	0.0	0.0	0.0		0.0	0.0	0.0	0.0
35.4	33.4	26.7	21.3		36.7	37.3	39.0	33.6
35.4	33.4	26.7	21.3		36.7	37.3	39.0	33.6
117.6	398.5	743.2	686.0		1794.1	1303.9	1925.9	1111.3
117.6	398.5	743.2	686.0		1794.1	1303.9	1925.9	1111.3
517.9	704.1	1018.9	966.7		1889.6	1408.5	2064.8	1292.3
517.9	704.1	1018.9	966.7		1889.6	1408.5	2064.8	1292.3
599.5	910.5	1242.2	1192.3		2124.5	1499.2	2275.6	1401.5
599.5	910.5	1242.2	1192.3		2124.5	1499.2	2275.6	1401.5
897.8	1185.9	1522.9	1471.2		2409.6	1788.2	2524.0	1663.7
897.8	1185.9	1522.9	1471.2		2409.6	1788.2	2524.0	1663.7
1979.7	2365.9	2506.8	2583.2		2564.3	2026.8	2909.3	1901.3
1979.7	2365.9	2506.8	2583.2		2564.3	2026.8	2909.3	1901.3
2008.1	2392.0	2534.6	2618.1		2772.4	2221.6	3047.4	2043.2
2008.1	2392.0	2534.6	2618.1		2772.4	2221.6	3047.4	2043.2
5583.4	4964.2	4912.8	4870.3		5022.6	2338.9	5057.4	2093.0
5583.4	4964.2	4912.8	4870.3		5022.6	2338.9	5057.4	2093.0
5606.7	4987.6	4937.9	4912.1		5056.3	2475.5	5097.7	2235.8
5606.7	4987.6	4937.9	4912.1		5056.3	2475.5	5097.7	2235.8
6524.6	5695.0	5682.4	5604.4		6111.5	3717.9	6020.4	3170.7
6524.6	5695.0	5682.4	5604.4		6111.5	3717.9	6020.4	3170.7
6911.7	5990.0	5931.4	5842.9		6380.0	3979.5	6270.0	3374.5
6911.7	5990.0	5931.4	5842.9		6380.0	3979.5	6270.0	3374.5
7321.1	6452.9	6508.7	6435.6		7156.3	4568.8	7145.4	4164.0
7321.1	6452.9	6508.7	6435.6		7156.3	4568.8	7145.4	4164.0
7680.4	6731.0	6743.7	6673.8		7390.9	4797.0	7358.2	4334.1
7680.4	6731.0	6743.7	6673.8		7390.9	4797.0	7358.2	4334.1
Calculated main values of the *g* tensor (g_X, g_Y, g_Z) of the ground manifold (pseudospin *S*=1/2)								
1.068	1.716	4.847	5.145		1.470	1.999	1.386	2.081
1.809	2.865	4.533	4.313		2.031	3.668	1.863	3.931
9.012	6.705	2.121	2.087		6.549	5.938	6.612	5.878

Molecule 2 (Fe-C bond 1.99872 Å)

CASSCF energies of the low-lying spin quintets (S=3/2). All doublets and sextets are much higher in energy.								
SZ	SZ	SZ	SZ		DZP	DZP		
CAS (7,5)	CAS (7,7)	CAS (11,9)	CAS (15,13)		CAS (7,5)	CAS (7,10)		
0	0	0	0		0	0		
255	927	1311	1262		2445	1521		
352	962	1345	1293		2597	1945		
1768	2370	2532	2618		2699	2059		
5294	4805	4767	4717		5104	2215		
6777	5819	5731	5626		6449	3916		
6969	6263	6358	6288		7268	4531		
CASSCF / RASSI-SO energies of the low-lying spin-orbit states								
0.0	0.0	0.0	0.0		0.0	0.0		
0.0	0.0	0.0	0.0		0.0	0.0		
69.7	29.2	27.5	21.0		37.8	41.1		
69.7	29.2	27.5	21.0		37.8	41.1		
144.1	648.0	1011.4	959.2		2250.9	1402.5		
144.1	648.0	1011.4	959.2		2250.9	1402.5		
531.2	932.8	1276.2	1228.6		2355.7	1502.8		
531.2	932.8	1276.2	1228.6		2355.7	1502.8		
682.8	1155.4	1501.8	1457.4		2428.8	1808.4		
682.8	1155.4	1501.8	1457.4		2428.8	1808.4		
968.9	1434.7	1786.6	1739.7		2752.1	1999.6		
968.9	1434.7	1786.6	1739.7		2752.1	1999.6		
2019.5	2484.9	2631.1	2702.7		2922.1	2195.8		
2019.5	2484.9	2631.1	2702.7		2922.1	2195.8		
2049.7	2509.7	2661.3	2740.0		3129.9	2343.9		
2049.7	2509.7	2661.3	2740.0		3129.9	2343.9		
5542.1	4921.3	4862.5	4813.6		5192.4	2426.9		
5542.1	4921.3	4862.5	4813.6		5192.4	2426.9		
5565.5	4946.4	4889.7	4856.2		5230.9	2604.3		
5565.5	4946.4	4889.7	4856.2		5230.9	2604.3		
6521.3	5608.4	5568.0	5474.6		6253.0	3768.8		
6521.3	5608.4	5568.0	5474.6		6253.0	3768.8		
6900.4	5875.7	5786.4	5679.4		6498.4	3997.9		
6900.4	5875.7	5786.4	5679.4		6498.4	3997.9		
7325.5	6421.9	6480.5	6406.7		7386.3	4687.4		
7325.5	6421.9	6480.5	6406.7		7386.3	4687.4		
7676.6	6671.9	6684.8	6610.9		7598.1	4886.5		
7676.6	6671.9	6684.8	6610.9		7598.1	4886.5		
Calculated main values of the g tensor (g_X, g_Y, g_Z) of the ground manifold (pseudospin S=1/2)								
0.397	5.160	5.358	1.870		1.683	1.690		
0.550	4.339	3.779	3.129		2.584	2.657		
8.967	2.096	2.042	5.919		6.149	6.614		

References:

(S1) (a) Stalke, D. *Chem. Soc. Rev*. **1998**, *27*, 171-178. (b) Kottke, T.; Stalke, D. *J. Appl. Crystallogr.* **1993**, *26*, 615-619.

(S2) Schulz, T.; Meindl, K.; Leusser, D.; Stern, D.; Graf, J.; Michaelsen, C.; Ruf, M.; Sheldrick, G. M.; Stalke, D. *J. Appl. Crystallogr*. **2009**, *42*, 885-891.

(S3) SAINT, Bruker AXS Inc., Madison, Wisconsin (USA) 2000.

(S4) Sheldrick, G. M. *SADABS*, Universität Göttingen, Germany, 2000.

(S5) (a) Sheldrick, G. M. *Acta Crystallogr*., Sect. A **1990**, *46*, 467−473. (b) Sheldrick, G. M. *Acta Crystallogr*., Sect. A **2008**, *64*, 112−122. (c) Müller, P.; Herbst-Irmer, R.; Spek, A. L.; Schneider, T. R.; Sawaya, M. R. In *Crystal Structure Refinement−A Crystallographer's Guide to SHELXL, IUCr Texts on Crystallography*; P. Müller, Ed.; Oxford University Press: Oxford, U.K., 2006; Vol. 8. (d) Hübschle, C. B.; Sheldrick, G. M.; Dittrich, B. *J. Appl. Crystallogr*. **2011**, *44*, 1281−1284

(S6) Hashimoto, T.; Urban, S.; Hoshino, R.; Ohki, Y.; Tatsumi, K.; Glorius, F. *Organometallics*, **2012**, *31*, 4474−4479. (S8) Parsons, S.; Flack, H. D.; Wagner, T. *Acta Cryst.* **2013**, *B69*, 249-259.

(S7) *Mfit* program: E. Bill, Max-Planck Institute for Chemical Energy Conversion, Mülheim/Ruhr, Germany.

(S8) *julX* program: E. Bill: Max-Planck Institute for Chemical Energy Conversion, Mülheim/Ruhr, Germany.

(S9) (a) Cage, B.; Hassan, A. K.; Pardi, L.; Krzystek, J.; Brunel, L.-C.; Dalal, N.S. *J. Magn. Reson.* **1997**, *124*, 495-498. (b) van Tol, J.; Brunel, L.-C.; Wylde, R.J. *Rev. Sci. Instrum.* **2005**, *76*, 074101. (c) Morley, G.W.; Brunel, L.-C.; van Tol, J. *Rev. Sci. Instrum.* **2008**, *79*, 064703.

(S10) Weil, J. A.; Bolton, J. R., *Electron Paramagnetic Resonance Elementary Theory and Practical Applications, 2nd ed.* Wiley−Interscience: Hoboken, NJ, **2007**, Chapter 6.

(S11) Kortz, U.; Muller, A.; van Slagren, J.; Schnack, J.; Dalal, N.S.; Dressel, M. *Coord. Chem. Rev***. 2009**, *253*, 2315–2327.

(S12) (a) Krzystek, J.; Ozarowski, A.; Telser, J.; *Coord. Chem. Rev*. **2006**, *250*, 2308‑2324. (b) Krzystek, J.; Zvyagin, S.A.; Ozarowski, A.; Trofimenko, S.; Telser, J. *J. Magn. Reson*, **2006**, *178*, 174‑183.

(S13) Aquilante, F.; Vico, L. D.; Ferré, N.; Ghigo, G.; Malmqvist, P.-Å.; Neogrády, P.; Pedersen, T. B.; Pitonak, M.; Reiher, M.; Roos, B. O.; Serrano-Andrés, L.; Urban, M.; Veryazov V.; Lindh, R.; *J. Comput. Chem*., **2010**, *31*, 224-247.

(S14) Abragam, A.; Bleaney, B., *Electron Paramagnetic Resonance of Transition Ions.* Oxford Press: Oxford, United Kingdom, **1970**.